Linear coupling of patterning systems can have nonlinear effects

N. Mahashri[1], Thomas E. Woolley[2], and M. Chandru[1]*
[1] *Department of Mathematics, School of Advanced Sciences, Vellore Institute of Technology, Vellore 632014 and*
[2] *Cardiff School of Mathematics, Cardiff University, Senghennydd Road, Cardiff CF24 4AG, UK*
(Dated: January 8, 2025)

Isolated patterning systems have been repeatedly investigated. However, biological systems rarely work on their own. This paper presents a theoretical and quantitative analysis of a two-domain interconnected geometry, or bilayer, coupling two two-species reaction-diffusion systems mimicking interlayer communication, such as in mammary organoids. Each layer has identical kinetics and parameters, but differing diffusion coefficients. Critically, we show that despite a linear coupling between the layers, the model demonstrates nonlinear behaviour; the coupling can lead to pattern suppression or pattern enhancement. Using the Routh-Hurwitz stability criterion multiple times we investigate the pattern forming capabilities of the uncoupled system, the weakly coupled system and the strongly coupled system, using numerical simulations to back up the analysis. We show that although the dispersion relation of the entire system is a non-trivial octic polynomial the patterning wave modes in the strongly coupled case can be approximated by a quartic polynomial, whose features are easier to understand.

I. INTRODUCTION

The formation of complex biological structures, from tissues to embryos, depends on a wide variety of morphogenetic mechanisms. Various mathematical frameworks have been developed [1] to explain such autonomous self-organisation, with diffusion-driven instabilities, or Turing mechanisms, being one of the most widely applied ideas [2].

Although Turing patterns have been suggested to be behind the patterning of various natural systems, such as animal coat markings, teeth, hair follicles, feather placodes, and fingerprints [3–7], the existence of Turing patterns has only been demonstrated categorically and mathematically analysed in chemical systems [8].

Most mathematical investigations into pattern formation use the basic components of two interacting and diffusing populations in simple geometries [9–11]. However, biological systems rarely work in isolation. From simple biological cases of mammary organoids (which are formed of two layers of interconnected cells [12]) to complex cases such as neural [13], biochemical [14], or ecological networks [15], there may exist multiple interconnected, communicating layers. Moreover, each layer may have distinct qualities that differentiate it from the others, requiring effective integration for the smooth operation of the system.

Here, we focus on investigating the effects of linearly coupling two geometric domains similar to [16, 17], which we refer to as a bilayer. Each layer is a finite one-dimensional straight line and each layer will have its own independent system of components that are able to generate heterogeneous spatial patterns. We will demonstrate that linear coupling between the systems can have nonlinear effects, such as pattern suppression, or pattern enhancement. Critically, the term bilayer may have different interpretations in other literature [18].

Prior research has investigated a variety of layered coupled systems that generate a wide spectrum of spatiotemporal patterns [16, 17, 19–22]. In a study conducted by Berenstein (2004) [20], the presence of superlattice patterns in a bilayer coupled system was experimentally confirmed. The analysis of the bilayer coupled CDIMA system, considering the effects of illumination, was also conducted in [21, 22] highlighting how external effects can influence the system.

In contrast to [16], which focused on a bilayer linearly coupled system with distinct layers resulting from different parameters, [17] examined a bilayer linearly coupled system with identical layers (i.e., the same kinetics parameters) and varied interlayer diffusion coefficients. Although our interests are similar, [17] focused on a system in which patterns only existed for a small range of the coupling strength, whereas our system presents the opposite phenomena, in that patterns exist for all coupling strengths beyond a critical value.

Konishi (2018) [23] also examined the influence of bilayers on linearly coupled patterning systems. However, their focus was on patterns that had the same wavelength in each layer, whilst we consider patterns of different wavelengths. In the context of stability analysis, Catllá (2012) [24] investigated the stability of homogeneous steady states within a bilayer linearly coupled system characterised by identical layers, akin to our own by the utilisation of the block symmetric structure to the linear problem. In contrast, we proceed with a one-dimensional examination of our system and confirm its

* Correspondence email address: leochandru@gmail.com

stability by applying the Routh-Hurwitz (RH) stability criterion.

Numerous physical, or biological systems, such as the Faraday three-wave experiments [25, 26], bacteria growth on an agar substrate [27], the bilayer structure of embryonic skin [5–7], and bulk chemotaxis [18], have prompted researchers to explore coupled systems of reaction-diffusion models. Likewise, a bilayer biological model, like the one depicting the transmission of brain tumours from one layer of brain tissue to the other, has generally consisted of two equations, one for the transmission of tumours in grey matter and one for the transmission in white matter [28]. However, comprehending each distinct layer in a coupled system does not imply a comprehensive understanding of the entire system. It is essential to recognise that homogenization arguments may not always be suitable [29].

In addition to the biological implications, there is a mathematical justification for considering bilayers. One way to model 2D Turing patterns is to discretise them into a grid of points, which looks like a network of interconnected 1D layers. Thus, although we know that patterns can be supported by the linear coupling process, we do not know how this coupling can influence the patterns.

In this paper we do not consider a specific application. Instead, we follow a more theoretical approach providing a proof of existence of nonlinear dynamics driven by linear coupling. As such, we keep the pattern forming populations general and call them 'morphogens'. The coupling strength, η, refers to the rate at which the morphogens or species populations are transferred between the different layers. Besides the linear coupling that we are going to consider, other methods such as dynamic coupling [19], coupling with delays [30], and nonlinear coupling [31, 32] have also been investigated.

The researchers in [31] studied a bilayer non-linearly coupled system and discovered that the pattern becomes more apparent as the coupling strengths increase. Put simply, the only pattern that remains is the one with the longest wavelength. Also, the authors of [32] have demonstrated the impact of long wavelength mode on short wavelength mode in bilayer coupled systems. They observed that in the case of non-linear coupling, this influence increases and the intensity ratio of the two Turing modes changes with the coupling parameter.

In the field of nonlinear research, it has been demonstrated that two nonlinear oscillators, can exhibit a quenching phenomenon known as amplitude death, which signifies the suppression of oscillation [33]. In addition, it has been demonstrated that Turing-type bifurcations can bring about a transition from amplitude death to oscillation death [34, 35].

Motivated by the aforementioned papers on wavelengths and building upon the earlier discourse regarding the biological aspect of tumour growth across layers, we explore the results of a bilayer linearly coupled system with varying interlayer diffusion coefficients providing considerably different wavelengths for both layers. This study emphasises the coupling of two distinct layers and demonstrates that linear coupling can generate similar behaviours observed in non-linearly coupled systems. We demonstrate that the patterns can be inhibited by weak coupling and reformed by strong coupling. Significantly, the wave mode of the combined system is a weighted combination of both system's wave modes, rather than one system dominating the other.

The outline of the manuscript is as follows: Section II describes the bilayer linearly coupled system, detailing the specific kinetics and parameters employed. Section III presents the specifics of the numerical simulations performed. Sections IV to VI examine stability in detail. Section VII explores the physical insights of nonlinear behaviour. Section VIII concludes with an extensive overview and discussion, aiming to elucidate its dynamic nature. Those familiar with linear stability analysis for large numbers of populations may concentrate on the findings presented in Section VII and the subsequent discussion in Section VIII.

II. METHODS - TWO SPECIES

Since Turing's seminal article and the later rediscovery of the short-range activation and long-range inhibition by Gierer & Meinhardt [36], a progressive wealth of theory has focused on reaction-diffusion systems as a model for pattern formation [3].

Fundamentally, we say that a system of reaction-diffusion equations is able to undergo a Turing instability if the morphogen populations have a spatially homogeneous steady state in the absence of population diffusion, which can be driven unstable when population diffusion is included. Generally, the Turing analysis considers a system of two nonlinearly interacting morphogen populations in a simply connected spatial domain of dimension less than or equal to three [37]. Here, we extend this notion to consider multiple interacting systems of the same species.

We consider two one-dimensional spatial domains characterised by a nondimensional length of $x \in [0, 130]$. On each layer, we define two morphogen populations, u_i and v_i, where $i = 1$, or 2, indicates the morphogen's layer. These populations undergo reaction-diffusion dynamics in their own layer and are able to transfer be-

tween layers, as defined by the system

$$\frac{\partial u_1}{\partial t} = \frac{\partial^2 u_1}{\partial x^2} + f(u_1, v_1) + \eta(u_2 - u_1), \tag{1}$$

$$\frac{\partial v_1}{\partial t} = D_1 \frac{\partial^2 v_1}{\partial x^2} + g(u_1, v_1) + \eta(v_2 - v_1), \tag{2}$$

$$\frac{\partial u_2}{\partial t} = D_2 \frac{\partial^2 u_2}{\partial x^2} + f(u_2, v_2) + \eta(u_1 - u_2), \tag{3}$$

$$\frac{\partial v_2}{\partial t} = D_3 \frac{\partial^2 v_2}{\partial x^2} + g(u_2, v_2) + \eta(v_1 - v_2), \tag{4}$$

where D_1, D_2 and D_3 are the positive nondimensionalised diffusion coefficients (refer Appendix A) and η is the coupling strength. η is a positive constant whose bounds are not restricted by any particular physical or biological application; rather, we restrict η to the interval $[0, 10]$ because significant changes in the patterns' behaviour are noticed within this range. Beyond this range, the coupling is so strong that the u and v populations become equal in each layer. Equations (1)-(4) are supplemented with no-flux boundary conditions and small random perturbations about the homogeneous steady states (that we assume exist) as initial conditions.

For clarity, we use the Schnakenberg kinetics [38] in their non-dimensional form (refer to Appendix A) given by

$$f(u, v) = a - u + u^2 v, \tag{5}$$

$$g(u, v) = b - u^2 v, \tag{6}$$

where, unless otherwise stated, $a = 0.05$, $b = 1.4$, $D_1 = 50$, $D_2 = 40$, and $D_3 = 800$ are taken as the reaction kinetics parameters and diffusion coefficients for both layers, ensuring that the same steady states are available in both layers. Our interests stem from varying the diffusion coefficients between the layers. Thus, when uncoupled ($\eta = 0$) the morphogens in both layers can pattern independently and present patterns of different wavelengths.

We proceed as generally as possible, however, there comes a point at which the algebra becomes intractable and we depend on numerical simulation to provide clarity. Although the outcomes presented in this study are tailored to our particular case, we offer the relevant codes at `https://github.com/mahaksn/Linear-Coupling`, enabling interested readers to efficiently replicate our algebraic manipulations and simulations with their own systems of interest.

III. NUMERICAL SIMULATIONS

In the context of simulating reaction-diffusion systems, the implicit-explicit (IMEX) scheme is acknowledged for its enhanced efficiency [39, 40]. This is because it facilitates unconditional stability in the diffusion term through the implicit scheme, while simultaneously supporting the nonlinearity of the reaction term via the explicit scheme.

Consequently, we adopt the implicit Crank-Nicolson method (which is numerically stable, even when subjected to the influence of noise [41, 42]) to address the diffusion term. Further, the Crank-Nicolson method is recognised for its consistency and unconditional stability within the L^2 norm, serving as a finite difference scheme for partial differential equations that converges in accordance with the Lax Equivalence theorem [43]. In contrast, the explicit Euler method is used to update the reaction terms [44].

The spatial domain, characterised by a nondimensional length of $L = 130$, is discretised into $n_x = 200$ equidistant nodes, and numerical simulations are executed with a time step not exceeding $\Delta t = 0.01$ (in nondimensionalised time units). However, convergence has been tested through simulations using finer spatial and temporal scales (refer to Appendix B).

In terms of termination condition, we effectively put a threshold on the time derivative. Namely, if we define $\boldsymbol{u}_x^t = (u_{1,x}^t, v_{1,x}^t, u_{2,x}^t, v_{2,x}^t)$ to be the solution state at the spatially discretised node x and at time t then the solution is iterated over time, t, until the difference between two iterations is less than 10^{-7}, namely, $\max_x(||\boldsymbol{u}_x^{t+1} - \boldsymbol{u}_x^t||) < 10^{-7}$, resulting in a stable final pattern.

To demonstrate the result we are examining, we conduct simulations of equations (1)-(4) using kinetics (5) and (6) while gradually increasing the values of η. Note that the v population in each layer has the same frequency as the u population in its layer, but is out of phase with u, so we only visualise the u population in each layer.

As depicted in Fig. 1, when η is small, the populations of u in the two layers exhibit distinct patterning frequencies. By the time $\eta = 0.07$, we begin to observe that the patterns start to influence each other since there is a noticeable phase shift in u_2, although there is no significant change in u_1. As η increases, the pattern vanishes entirely. Nevertheless, when the coupling strength increases, the pattern resurfaces with a single frequency across all populations.

Throughout the remainder of this paper, we endeavour to comprehend this non-linear phenomenon, which stems from linear coupling. We examine our linearized system around the steady states in Sections IV and V. These sections are designed for a standard Turing patterning system with two layers that have similar kinetics and parameters. In Section VI, we thoroughly examine our system's instability region using numerical evidence, offering insights into the patterning regime. Section VII concludes with the identification of the mode values in the weak coupling and strong coupling regions, which

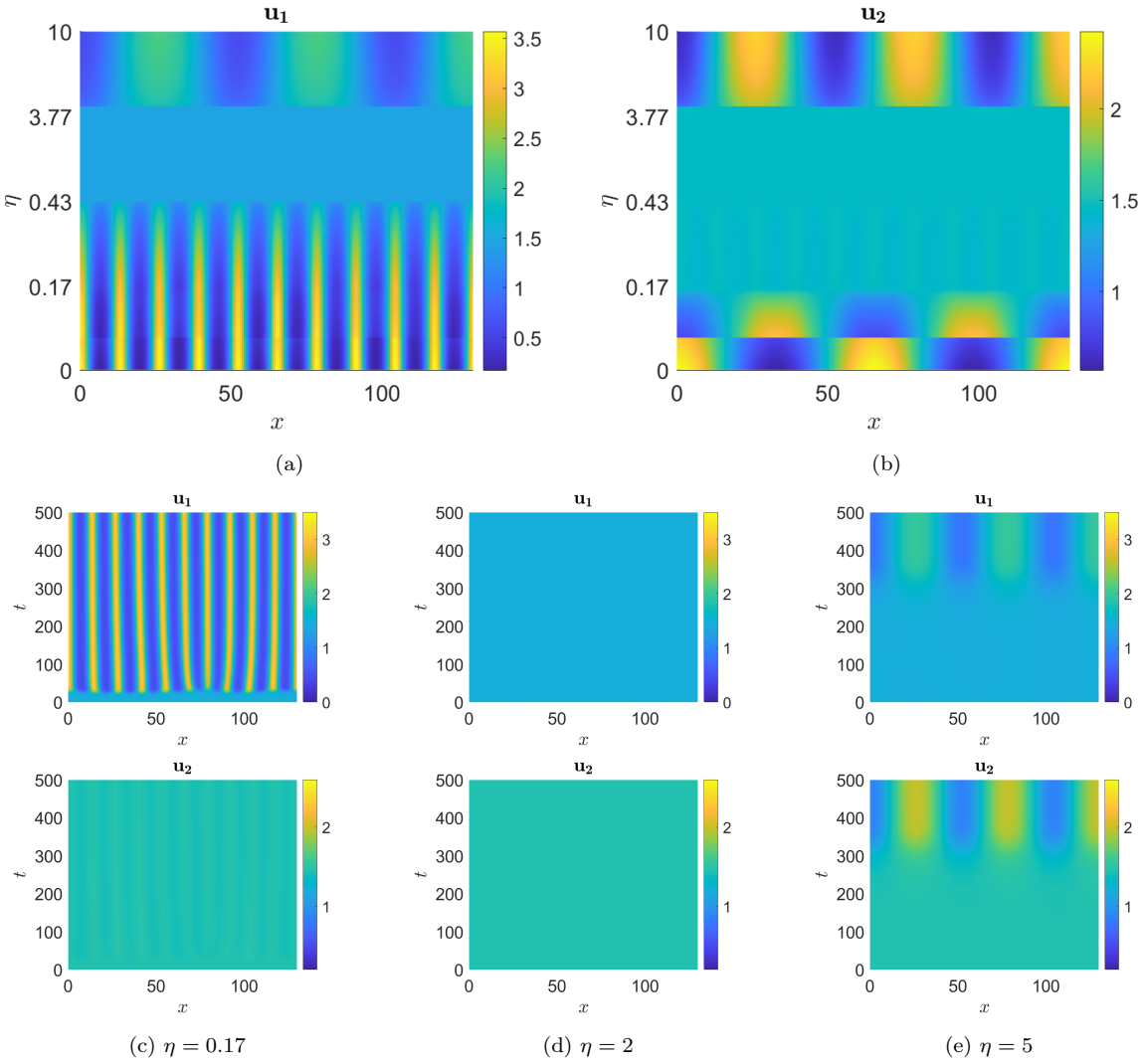

Figure 1: Change in the pattern of (a) u_1 and (b) u_2 as η increases. For smaller η values, 9 wavelengths of u_1 are visible, whilst 2 wavelengths of u_2 are visible, which disappear as η increases. For $\eta > 3.77$, only 2.5 wavelengths reappear. The pattern transition of v_i is in out-phase to u_i. Evolution of patterns of u_1 and u_2 at (c) $\eta = 0.17$, (d) $\eta = 2$ and (e) $\eta = 5$.

contribute to a better understanding of the nonlinear effect caused by linear coupling.

IV. LINEAR STABILITY ANALYSIS WITHOUT INTERLAYER COUPLING

When dealing with systems with multiple layers, direct linear analysis is challenging due to the fact that the criterion for patterning instability is a polynomial of high order. Here, we consider the uncoupled systems, $\eta = 0$, thus, we can directly apply well-known Turing analysis to the two two-species systems separately.

Given the specified conditions, the populations on each layer reach a state of equilibrium with a steady state, $\boldsymbol{u}_{i_0} = (a+b, b/(a+b)^2)$. Perturbing these states, we consider the evolution of a trajectory of the form

$$\boldsymbol{u}_i = \boldsymbol{u}_{i_0} + \boldsymbol{\epsilon}_i, \tag{7}$$

where $\boldsymbol{u}_i = (u_i, v_i)^T$ and $\boldsymbol{\epsilon}_i$ represents a small perturbation of the form $\boldsymbol{\epsilon}_i = \boldsymbol{\omega}_i \exp(\lambda t)$, where $\boldsymbol{\omega}_i = (\omega_{u_i}, \omega_{v_i})^T$ and $0 < |\omega_{u_i}| \ll 1$, $0 < |\omega_{v_i}| \ll 1$. The parameter λ is a constant that is determined through a consistency condition. Its sign indicates the stability of the system.

Due to the common nature of the linear analysis in the two-species case [1] we relegate the details to appendices C I and C II, where we show that the steady state is stable in the absence of diffusion when

$$\frac{b-a}{a+b} - (a+b)^2 < 0, \tag{8}$$

but unstable in the presence of diffusion when

$$(a+b)^4 - 2d_i(a+3b)(a+b) + d_i^2\left(\frac{a-b}{a+b}\right)^2 > 0, \quad (9)$$

where $d_1 = D_1$, and $d_2 = D_3/D_2$. Note that the parameter region is known not to be empty for appropriate ratios of d_i [45]. Also note that, as a final restriction for generating a pattern, the domain needs to be 'large enough' to allow the pattern to form, see Section C II for further details. We will always assume that this is the case, as we are focusing on the role of the coupling strength in this problem, rather than the influence of the geometry.

Critically, the analysis in appendices C I and C II depends on at most quadratic equations. However, in upcoming sections, we will be investigating quartic and octic polynomials. To ascertain the stability of a linear system in such higher degree cases, we will use the Routh-Hurwitz (RH) stability criterion multiple times. In summary, the RH criterion allows us to understand the sign of λ without explicitly calculating it, which provides a method of investigating whether a patterning instability is possible in cases where the characteristic polynomial is of high degree. Although the RH criterion can be applied to a polynomial of any degree, we provide a comprehensive explanation of the criterion in Appendix D for quartic polynomials that will prove valuable in the subsequent sections. Helpfully, the octic polynomials will be transformable into quartic polynomials through judicious reparametrisation.

V. LINEAR STABILITY WITH COUPLING, BUT WITHOUT DIFFUSION

Here, we repeat the linear analysis but include the coupling between the layers. We note that in the absence of diffusion, we want the coupled system to have a stable homogeneous steady state.

When equation (7) is substituted into the system

$$\frac{du_i}{dt} = f(u_i, v_i) + \eta(u_j - u_i), \quad (10)$$

$$\frac{dv_i}{dt} = g(u_i, v_i) + \eta(v_j - v_i), \quad (11)$$

where $\boldsymbol{\epsilon}_i = \boldsymbol{\omega}_i \exp(\lambda t)$, we get

$$(\lambda \mathbf{I}_4 - \mathbf{J}_0 - \eta \mathbf{C}) \begin{bmatrix} \boldsymbol{\omega}_1 \\ \boldsymbol{\omega}_2 \end{bmatrix} = \mathbf{0}, \quad (12)$$

where I_n is the $n \times n$ identity matrix of order n

$$\mathbf{J}_0 = \begin{bmatrix} \mathbf{J} & \mathbf{0} \\ \mathbf{0} & \mathbf{J} \end{bmatrix}, \quad \mathbf{C} = \begin{bmatrix} -\mathbf{I}_2 & \mathbf{I}_2 \\ \mathbf{I}_2 & -\mathbf{I}_2 \end{bmatrix},$$

and $\mathbf{J}$ is given in Appendix C I, equation (C4). Equation (12) only has a nontrivial solution is the prefactor matrix is singular, meaning that its determinant is zero. The determinant is a quartic function in λ, which also has a dependence on η and can be expressed as:

$$y(\lambda, \eta, 0) = \lambda^4 + \sum_{n=0}^{3} y_{n_0}(\eta)\lambda^n, \quad \eta > 0, \quad (13)$$

where

$$\begin{aligned} y_{3_0} &= 4\eta - 2c_1, \\ y_{2_0} &= 4\eta^2 - 6\eta c_1 + c_1^2 + 2c_2, \\ y_{1_0} &= -4\eta^2 c_1 + 2\eta(c_1^2 + 2c_2) - 2c_1 c_2, \\ y_{0_0} &= 4\eta^2 c_2 - 2\eta c_1 c_2 + c_2^2, \end{aligned}$$

where c_1 and c_2 are given by equations (C5) and (C6), respectively.

Since equation (13) is a quartic polynomial we appeal to the RH criterion. After constructing the Routh array (as explained in the Appendix D) we find that the real part of λ is negative if all coefficients y_{0_0} - y_{3_0} and

$$\begin{aligned} y_{\beta_0} &= 4\eta^2 - 5\eta c_1 + c_1^2 + c_2, \\ y_{\gamma_0} &= \tfrac{1}{y_{\beta_0}}\left[-2c_1(8\eta^4 - 14\eta^3 c_1 + \eta^2(7c_1^2 + 8c_2)\right. \\ &\quad \left. -\eta(6c_1 c_2 + c_1^3) + c_1^2 c_2)\right]. \end{aligned}$$

are positive. Since within the chosen Turing patterning region $c_1 < 0$ and $c_2 > 0$ then all of the y_{k_0} terms expressed here are positive (see Appendix E). Therefore, system (10) and (11) is stable with coupling in the absence of diffusion.

VI. LINEAR STABILITY WITH DIFFUSION AND COUPLING

We now find the patterning regime of our system with diffusion and coupling. Take $\boldsymbol{\epsilon}_i = \boldsymbol{\omega}_i \exp(\lambda t)\cos(kx)$, where $k = n\pi/L$ is the wave number with $n \in \mathbb{Z}$ that satisfies the no-flux boundary conditions on $[0, L]$. Substituting equation (7) into system (1)-(4) yields

$$(\lambda \mathbf{I}_4 + \mathbf{J}_\eta) \begin{bmatrix} \boldsymbol{\omega}_1 \\ \boldsymbol{\omega}_2 \end{bmatrix} = \mathbf{0}, \quad (14)$$

where $\mathbf{J}_\eta = k^2\mathbf{D} - \mathbf{J}_0 - \eta\mathbf{C}$ and $\mathbf{D} = diag(1, D_1, D_2, D_3)$. The dispersion relation is given by

$$y(\lambda, \eta, h) = \lambda^4 + \sum_{n=0}^{3} y_n(h, \eta)\lambda^n, \quad h = k^2, \quad (15)$$

where

$$
\begin{aligned}
y_3(h,\eta) &= h(c_3+c_4)+4\eta-2c_1,\\
y_2(h,\eta) &= h^2(c_3c_4+c_5+c_6)+h(3\eta(c_3+c_4)\\
&\quad -(c_1(c_5+c_6)+(c_8+c_9))\\
&\quad +(4\eta^2-6\eta c_1+(c_1^2+2c_2)),\\
y_1(h,\eta) &= h^3(c_3c_6+c_4c_5)+h^2(2\eta(c_3c_4+c_5+c_6)\\
&\quad -(c_1(c_5+c_6)+c_3c_9+c_4c_8))\\
&\quad +h(2\eta^2(c_3+c_4)-2\eta(c_1(c_3+c_4)\\
&\quad +(c_8+c_9))+(c_2(c_3+c_4)+c_1(c_8+c_9)))\\
&\quad +(-4\eta^2c_1+2\eta(c_1^2+2c_2)-2c_1c_2),\\
y_0(h,\eta) &= \sum_{l=0}^{4}\psi_l(\eta)h^l, \qquad (16)
\end{aligned}
$$

$$
\begin{aligned}
\psi_4(\eta) &= c_5c_6,\\
\psi_3(\eta) &= \eta(c_3c_6+c_4c_5)-(c_5c_9+c_6c_8),\\
\psi_2(\eta) &= \eta^2(c_5+c_6+c_7)-\eta(c_1(c_5+c_6)+c_3c_9+c_4c_8))\\
&\quad +(c_2(c_5+c_6)+c_8c_9),\\
\psi_1(\eta) &= -2\eta^2(c_8+c_9)+\eta(c_2(c_3+c_4)+c_1(c_8+c_9))\\
&\quad -c_2(c_8+c_9)),\\
\psi_0(\eta) &= 4\eta^2c_2-2\eta c_1c_2+c_2^2.
\end{aligned}
$$

The constants

$$
\begin{aligned}
c_3 &= 1+D_1,\\
c_4 &= D_2+D_3,\\
c_5 &= D_1,\\
c_6 &= D_2D_3,\\
c_7 &= D_3+D_2D_1.
\end{aligned}
$$

are all positive, given that the diffusion coefficients are positive constants. Likewise,

$$
\begin{aligned}
c_8 &= g_v+D_1f_u = c_{8,1},\\
c_9 &= D_2g_v+D_3f_u = D_2\times c_{9,2},
\end{aligned}
$$

where $c_{8,1}$ and $c_{9,2}$ are derived in equations (C15)-(C16) in Appendix C II and are seen to be positive.

A patterning instability occurs when λ has a positive real part. As explained in Appendix D, there cannot be a patterning instability unless at least one of the six RH conditions of equation (15),

$$
\begin{aligned}
RH1 &: y_3, && (17)\\
RH2 &: y_2, && (18)\\
RH3 &: y_1, && (19)\\
RH4 &: y_0, && (20)\\
RH5 &: y_{\beta_1} = \frac{y_2y_3-y_1}{y_3}, && (21)\\
RH6 &: y_{\gamma_1} = \frac{y_1y_2y_3-y_1^2-y_3^2y_0}{y_2y_3-y_1}, && (22)
\end{aligned}
$$

becomes negative.

Despite knowing the signs of all the constants involved, finding the exact parametric region of patterning is difficult because the space where the Turing patterns occur has six dimensions $(D_1, D_2, D_3, a, b, \eta)$. Consequently, in order to demonstrate the desired nonlinear behaviour, we use graphical methods to show the patterning regions for the given parameters. We determine the range of k and η within which the RH conditions become negative, thereby identifying the region in which $\lambda > 0$ (corresponding to the roots of the dispersion relation (15)) and, thus, a patterning instability can take place (see Fig. 2).

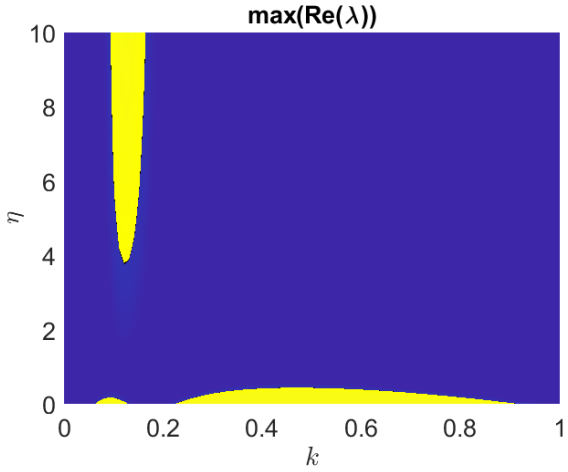

Figure 2: Sign plot of λ from equation (15). The blue region shows $\lambda < 0$ regions, and the patterning regime, or $\lambda > 0$, is shown by the yellow region.

We confirmed computationally that y_0 is the only component of the RH conditions of (15) (see Appendix F) which becomes negative for a particular region of (k, η) that provides the patterning region and information on the modes corresponding to the dispersion relation (Fig. 2). Figure 3 shows that the surfaces of y_3, y_2, y_1, y_β and y_γ never become negative while y_0 becomes negative (blue region) for a particular region of (k, η).

For better clarity and comparison, the sign plot of λ (Fig. 2) associated with the dispersion relation (15) is plotted alongside $y_0(k, \eta)$ (Fig. 3(d)) in Fig. 4, which emphasizes that it is the sign of y_0 that provides the necessary information for patterning. Observe that the longer wavelength loses its ability to pattern first followed by the shorter wavelength as η increases, which is corroborated in Fig. 5.

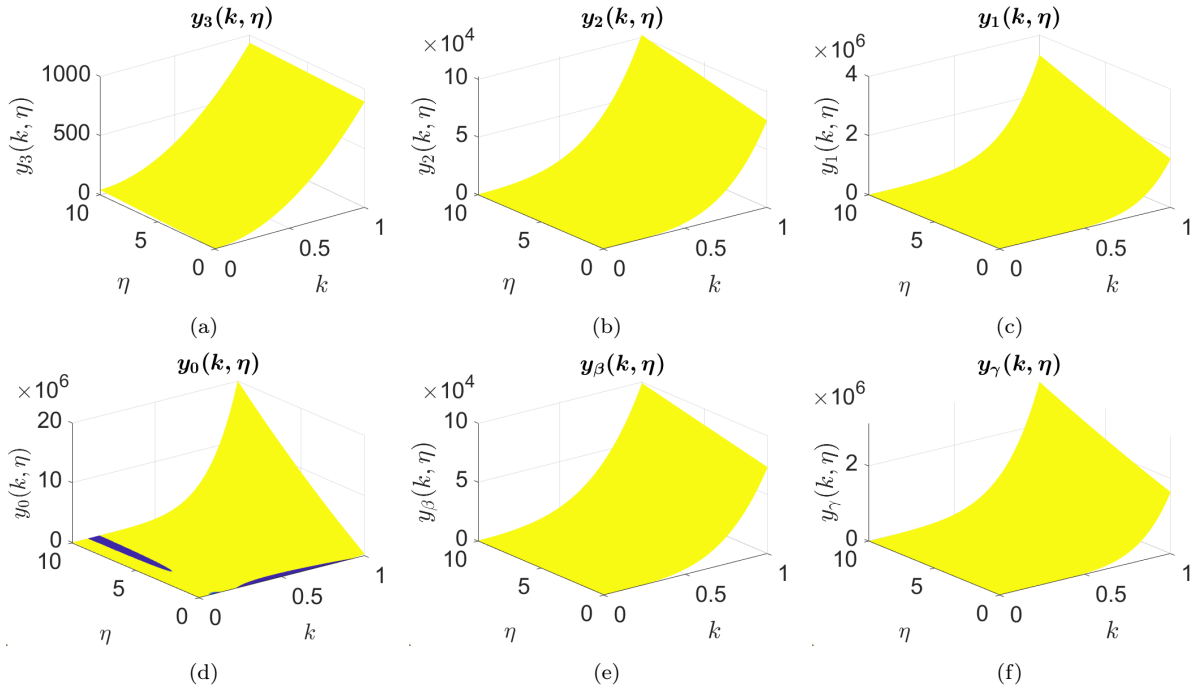

Figure 3: Surface plots of the RH conditions (17)-(22). The plots suggest that $y_0(k,\eta)$ is the only surface that becomes negative.

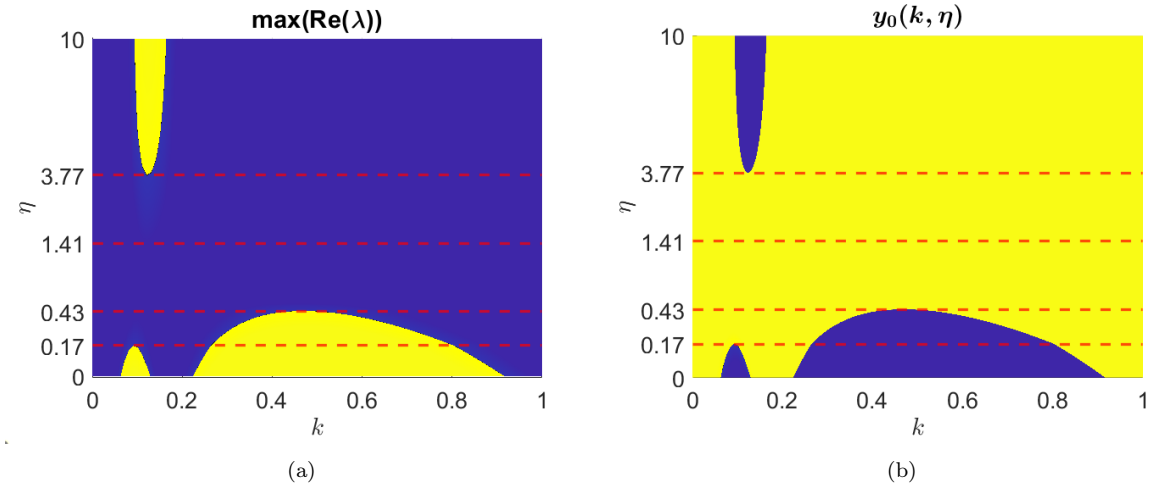

Figure 4: Sign plots of (a) λ from dispersion relation (15) and (b) y_0 from equation (16), where positive values are yellow and negative values are blue. The red dotted lines show the partitions highlighted in Table I.

VII. MODES

From the investigation in the last section, we have found that the sign of λ and therefore the stability of the homogeneous steady state depends solely on the sign of y_0. Since y_0 is a quartic function in h (see equation (16)) its discriminant is

$$\begin{aligned}\Delta_{y_0}(\eta) = {} & 256\psi_4^3\psi_0^3 - 192\psi_4^2\psi_3\psi_1\psi_0^2 - 128\psi_4^2\psi_2^2\psi_0^2 \\ & + 144\psi_4^2\psi_2\psi_1^2\psi_0 - 27\psi_4^2\psi_1^4 + 144\psi_4\psi_3^2\psi_2\psi_0^2 \\ & - 6\psi_4\psi_3^2\psi_1^2\psi_0 - 80\psi_4\psi_3\psi_2^2\psi_1\psi_0 \\ & + 18\psi_4\psi_3\psi_2\psi_1^3 + 16\psi_4\psi_2^4\psi_0 - 4\psi_4\psi_2^3\psi_1^2 \\ & - 27\psi_3^4\psi_0^2 + 18\psi_3^3\psi_2\psi_1\psi_0 - 4\psi_3^3\psi_1^3 \\ & - 4\psi_3^2\psi_2^3\psi_0 + \psi_3^2\psi_2^2\psi_1^2, \end{aligned} \tag{23}$$

which is a function of η that has the following four real roots, approximated to two decimal precision,

$$\eta_c = \{0.17, 0.43, 1.41, 3.77\}.$$

Although these are the critical coupling values that can produce different bifurcations, it is ultimately a question of whether there are any λ with a positive real part that drives the patterning (see the red lines on Fig. 4).

To investigate these parameter regions, we define P_i to be an interval delineated by values from η_c. In these partitioned intervals of η, the nature of the roots of y_0 are given in Table I.

Interval of η	**Number of real roots of equation** (16)	**Number of complex roots of equation** (16)
$P_1 = [0, 0.17]$	4	0
$P_2 = (0.17, 0.43]$	2	2
$P_3 = (0.43, 1.41)$	0	4
$P_4 = [1.41, 3.77)$	2	2
$P_5 = [3.77, 10]$	4	0

Table I: Nature of the roots of equation (16).

For the given set of parameters and a given η, it is nevertheless possible to determine the number of roots with positive real parts by applying the Routh-Hurwitz criterion to the polynomial y_0. Explicitly, the number of sign changes in the first column of the RH array (Table III) is equal to the number of roots with positive real parts. This means that in the partitioned intervals $(P_1, P_2, P_3, P_4, P_5)$ presented in Table I there are $(4, 2, 0, 0, 2)$ positive real k values, which are roots of equation (16). The number of roots of $y_0(k)$ then matches the number of roots of $\lambda(k)$, as visualised in Fig. 5, where we see the $\lambda(k)$ curve cutting the zero red dashed line the specified number of times.

For small coupling strengths $\eta \ll 0.17$, the two layers are effectively decoupled and the wave mode that appears in the simulations can be derived from the dispersion relation of the individual layers. For $\eta \in (0.17, 0.43)$, it is observed that only the shorter wavelength layer is capable of generating patterns and the wave mode values can still be determined approximately using the dispersion relation of this layer.

Figure 5 indicates that there are no positive eigenvalues for $\eta \in (0.43, 3.77)$. However, for $\eta > 3.77$, y_0 yields two positive real k roots and, thus, a pattern with a single wavelength is able to appear once again across the two layers (compare Figures 1, 4 and 5).

To get a handle on the large η features of the dispersion relation we investigate the shape of the curve y_0 (which we have shown drives the instability) after dropping the higher order terms of y_0 (see Fig. 6). Upon dropping the higher order terms we observe that the plot of the sign of y_0 is altered for small η and does not reproduce the patterning instability region well. However, in this parameter region, the two layers can be treated as approximately independent and are, thus, tractable. In contrast, the large η region is conserved across as the higher order terms are dropped (compare Figures 6(c) and 4(b)). By removing the insignificant terms from y_0, we obtain a solvable quadratic polynomial

$$y_{r_0}(h, \eta) = \sum_{l=0}^{2} \psi_l(\eta) h^l, \tag{24}$$

that approximates the required mode values for large coupling strengths, corresponding to the dispersion relation.

Consequently, our model demonstrates more intricate behaviours compared to the one discussed in [17]. Moreover, our findings stand in contrast to those of Li et al. (2015) [32], which indicate that the short wavelength mode is more susceptible to nonlinear coupling and ultimately vanishes, resulting in the persistence of only the long wavelength mode. In contrast, our investigation reveals that under conditions of linear coupling, the long wavelength mode is the first to disappear as the coupling strength is increased. After a brief period without any pattern formation, the long wavelength mode re-emerges as a single wavelength that is a combination of the two independent systems. Moreover, by illustrating that nonlinear behaviours can appear through linear coupling we have demonstrated that homogenization arguments that seek to reduce the complexity of coupled layers may not necessarily be sound, without clear analytic justification [29].

VIII. DISCUSSION AND CONCLUSION

For biological systems to operate efficiently, effective communication between multiple tissue layers is crucial, as each layer may have its own unique specifications. As an illustration, when it comes to the spread of brain tumours, the tumour tends to spread more rapidly across the grey matter compared to the white matter, highlighting the clear differentiation between these layers [29]. In order to gain a deeper comprehension of the underlying principles behind these processes, we devised a bilayer coupled system of reaction-diffusion equations. This system incorporates varying rates of diffusion in different layers while maintaining a linear diffusion between them. We employed Schnakenberg kinetics with a consistent set of parameters for both layers. Although the model had the same kinetics and was linearly coupled, it displayed nonlinear behaviour (Fig. 1).

At first, we conducted a linear analysis of our system to examine its behaviour around the steady states. This analysis was done directly using algebraic conditions

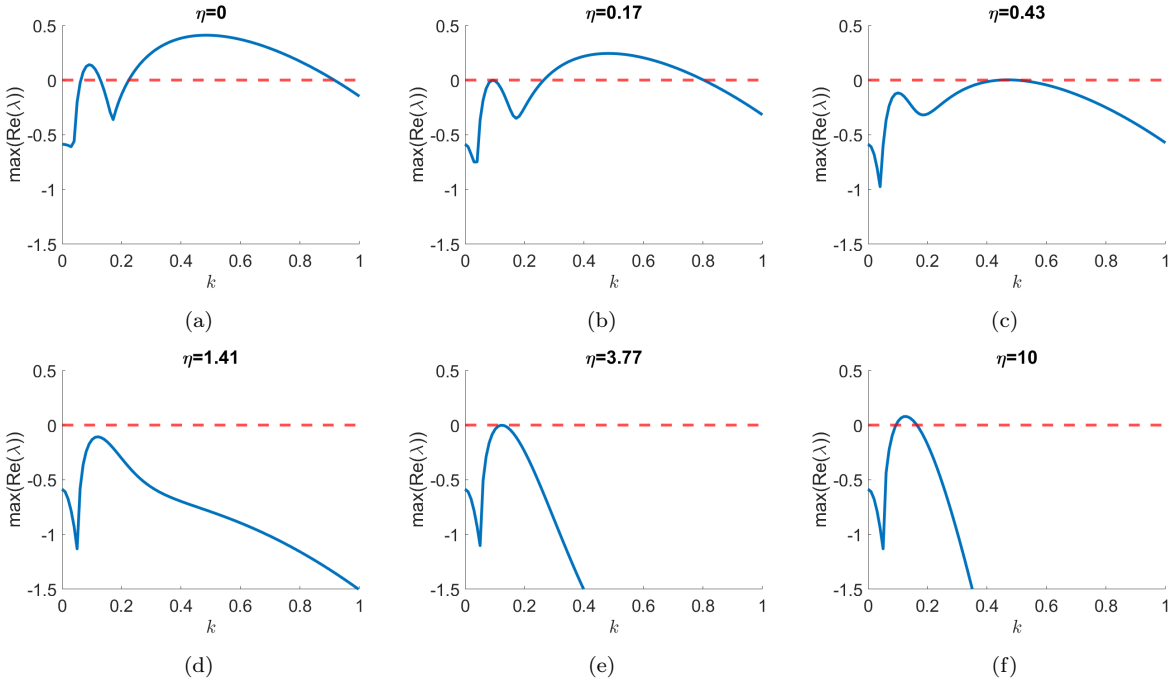

Figure 5: Dispersion curves for $\eta \in \eta_c$ illustrating the bifurcations occurring due to increasing η values.

through linearization for the separate layers. Critically, we choose parameter values then enable both layer to pattern separately, whilst the diffusion coefficients are selected to ensure two different pattern wavelengths. Since we needed to examine a quartic polynomial for both the coupled systems with and without diffusion, we applied the Routh-Hurwitz stability criterion to aid with the stability analysis.

Using the discriminant of y_0, equation (23), we were able to partition the range of η providing intervals of coupling strengths where different patterning dynamics were possible. The patterning modes of the system with weak coupling can be determined by analysing the dispersion relation of each layer separately. We approximated our dispersion relation through numerical experimentation by analysing y_0, equation (16), a quartic polynomial in h (octic in k). We were able to reduce the quartic polynomial y_0 to a lower order (quadratic) polynomial, which could be solved to get the mode values of the strongly coupled system. Therefore, we conducted a comprehensive analysis of our model to identify patterns in situations and regions that supported our assertion of nonlinear effects.

Our findings indicate that two primary parameter regimes contribute to pattern formation in the bilayer: one characterised by small η and the other by large η. We expect the two layers to pattern independently in the small η regime since they are effectively separate, which means that patterns of various wavelengths can be sustained. In contrast, under the large η regime, the spatial patterns remain consistent regardless of differences in the kinetic parameters between the two layers because the populations are effectively homogenised. This highlights a critical insight that even if we observe biological systems that have consistent patterns across multiple systems (e.g., the chemical and mechanical patterning aspects of fingerprint formation [7]), each patterning system may not be identical. Namely, it is possible that the coupling drives homogeneity of the patterns, rather than each system being developed identically. This mechanism would allow additional robustness to these biological systems as they would not be required to be made exactly the same during development, rather, the coupling of the systems would smooth out the heterogeneity between the systems.

With regards to the nonlinear phenomena that we have been considering it is important to question its generality regarding its existence in parameter space. Similar nonlinear behaviour (i.e., increasing η causing a disappearance and then reappearance of patterns) is observed when $a \in [0, 0.1]$ and $b \in [1.1, 1.95]$ are selected, ensuring that the initial homogeneous steady state (u_0, v_0) satisfies $u_0 \in [1.15, 1.95]$. As u_0 is adjusted from 1.15 to 1.95, the value of D_1 must change from 100 to 50. Subsequently, the values of D_2 and D_3 must vary such that ratio $\frac{D_1}{D_3/D_2}$ shifts from 6.5 to 1.25, with D_2 varying between 20 and 150 and D_3 ranging from 500 to 3000. Furthermore, the parameter D_2

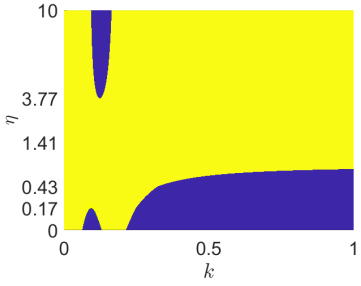

(a) Removed 4^{th} degree term in y_0, equation (16).

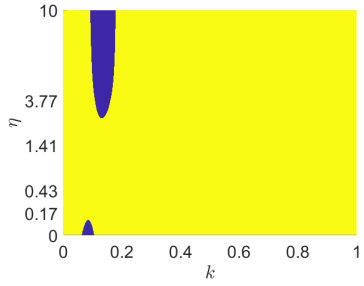

(b) Removed 3^{rd} degree term in y_0, equation (16).

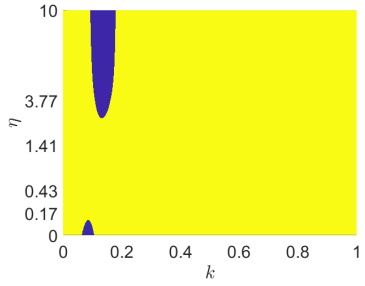

(c) Removed both 4^{th} and 3^{rd} degree terms in y_0, equation (16).

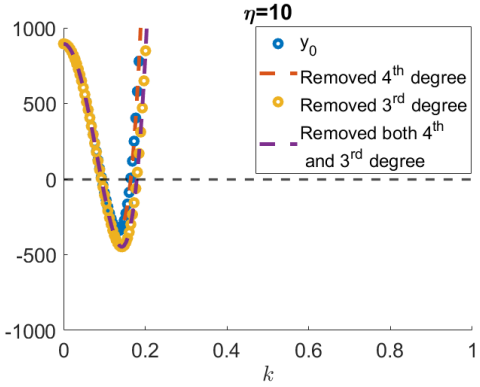

(d) Comparison graph

Figure 6: Graphs (a), (b), and (c) depict the changes in y_0 when the 4^{th} degree term, the 3^{rd} degree term, and both 4^{th} and 3^{rd} degree terms are eliminated, respectively. At the value of $\eta = 10$, the comparison graph of y_0 with (a), (b), and (c) is shown in (d). Here, it is noticeable that y_0 overlaps with the 4^{th} degree removed, while the 3^{rd} degree removed overlaps with both removed. Furthermore, it is evident that there is a minimal distinction between them as a whole.

should be smaller than D_1.

Thus, although the nonlinear phenomena exist in a nontrivial parameter space, other phenomena arising from the coupling are also possible (see Fig. 7). For example, in Fig. 7(a) the wave length of both layers collapses to one distribution for practically all η, so patterns always exist. Alternatively, it is also possible for the coupling to completely eradicate the pattern, as in Fig. 7(b).

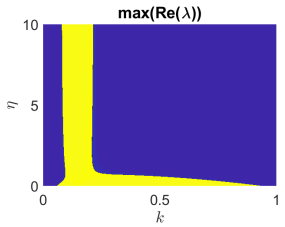

(a) $a = 0.05$, $b = 1.2$, $D_1 = 80$, $D_2 = 30$ and $D_3 = 600$.

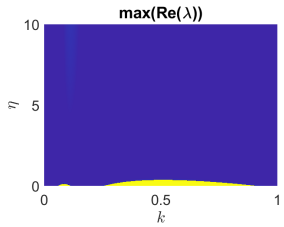

(b) $a = 0.05$, $b = 1.9$, $D_1 = 70$, $D_2 = 50$ and $D_3 = 1600$.

Figure 7: Sign plot of λ from equation (15) for the alternative scenarios other than Fig. 2.

It is imperative to acknowledge that this work serves as a proof-of-concept and does not aspire to achieve general applicability. Explicitly, as seen in Fig. 7, our investigation is only one part of a broader set of possible outcomes from the nonlinear coupling. Moreover, our research elucidates the core idea that the linear coupling of layers does not yield a linear outcome and the result stands in contrast to those previously discovered [17, 32]. Specifically, the integrated system exhibits a higher level of complexity than each of the constituent systems. Future work will explore the limits of complexity that can arise from a simple connection. For example, we plan to investigate our system by manipulating the wave number (k) between both layers.

Appendix A: Non-dimensionalization

Consider two one-dimensional spatial domains with two morphogen populations on each layer coupled to-

gether, represented by the system

$$\frac{\partial u_i}{\partial t} = D_{u_i}\frac{\partial^2 u_i}{\partial x^2} + f(u_i, v_i) + \eta(u_j - u_i), \tag{A1}$$
$$\frac{\partial v_i}{\partial t} = D_{v_i}\frac{\partial^2 v_i}{\partial x^2} + g(u_i, v_i) + \eta(v_j - v_i), \tag{A2}$$

where D_{u_i} and D_{v_i} are the respective positive diffusion coefficients with $i = 1$, or 2, indicating the morphogen's layer. Equations (A1) and (A2) are replaced with the generalised formulation of the Schnakenberg model [38], characterised as an activator-depleted substrate model

$$f(u, v) = k_1 a_1 - k_2 u + k_3 u^2 v, \tag{A3}$$
$$g(u, v) = k_4 b_1 - k_3 u^2 v, \tag{A4}$$

where the positive constants a_1, b_1, k_1, k_2, k_3, and k_4 are assumed to be the same across the two layers. At this juncture, we define

$$u_1 = [U_1]\bar{u}_1, \quad v_1 = [V_1]\bar{v}_1, \quad u_2 = [U_2]\bar{u}_2, \quad v_2 = [V_2]\bar{v}_2,$$
$$x = [L]\bar{x} \text{ and } t = [T]\bar{t},$$

where variables with over bars are dimensionless variables and the bracketed terms are dimensional scales, which we are free to choose. By substituting the aforementioned variables into equations (A1) and (A2) with kinetics (A3) and (A4), we obtain

$$\begin{aligned}
\frac{\partial \bar{u}_1}{\partial \bar{t}} &= D_{u_1}\frac{[T]}{[L]^2}\frac{\partial^2 \bar{u}_1}{\partial \bar{x}^2} + k_1 a_1 \frac{[T]}{[U_1]} - k_2[T]\bar{u}_1 \\
&\quad + k_3[U_1][V_1][T]\bar{u}_1^2\bar{v}_1 + \eta\left(\frac{[U_2]}{[U_1]}[T]\bar{u}_2 - [T]\bar{u}_1\right), \\
\frac{\partial \bar{v}_1}{\partial \bar{t}} &= D_{v_1}\frac{[T]}{[L]^2}\frac{\partial^2 \bar{v}_1}{\partial \bar{x}^2} + k_4 b_1 \frac{[T]}{[V_1]} - k_3[U_1]^2[T]\bar{u}_1^2\bar{v}_1 \\
&\quad + \eta\left(\frac{[V_2]}{[V_1]}[T]\bar{v}_2 - [T]\bar{v}_1\right), \\
\frac{\partial \bar{u}_2}{\partial \bar{t}} &= D_{u_2}\frac{[T]}{[L]^2}\frac{\partial^2 \bar{u}_2}{\partial \bar{x}^2} + k_1 a_1 \frac{[T]}{[U_2]} - k_2[T]\bar{u}_2 \\
&\quad + k_3[U_2][V_2][T]\bar{u}_2^2\bar{v}_2 + \eta\left(\frac{[U_1]}{[U_2]}[T]\bar{u}_1 - [T]\bar{u}_2\right), \\
\frac{\partial \bar{v}_2}{\partial \bar{t}} &= D_{v_2}\frac{[T]}{[L]^2}\frac{\partial^2 \bar{v}_2}{\partial \bar{x}^2} + k_4 b_1 \frac{[T]}{[V_2]} - k_3[U_2]^2[T]\bar{u}_2^2\bar{v}_2 \\
&\quad + \eta\left(\frac{[V_1]}{[V_2]}[T]\bar{v}_1 - [T]\bar{v}_2\right).
\end{aligned}$$

To simplify the system we choose,

$$[T] = \frac{[L]^2}{D_{u_1}}, \quad [U_1] = [V_1] = \beta_1, \quad [U_2] = [V_2] = \beta_2,$$

and combine the remaining parameters in the following dimensionless groupings

$$D_1 = \frac{D_{v_1}}{D_{u_1}}, \quad D_2 = \frac{D_{u_2}}{D_{u_1}}, \quad D_3 = \frac{D_{v_2}}{D_{u_1}}, \quad \gamma = \frac{k_2[L]^2}{D_{u_1}},$$
$$\beta_1 = \beta_2 = \sqrt{\frac{k_2}{k_3}}, \quad a = \frac{k_1 a_1\sqrt{\frac{k_3}{k_2}}}{k_2}, \text{ and } b = \frac{k_4 b_1\sqrt{\frac{k_3}{k_2}}}{k_2}.$$

Without loss of generality and to simplify the visualisation of the equations, we eliminate the over bars from the variables, resulting in a non-dimensional reaction-diffusion system characterised by a linear coupling of the general form

$$\frac{\partial u_1}{\partial t} = \frac{\partial^2 u_1}{\partial x^2} + \gamma(f(u_1, v_1) + \eta(u_2 - u_1)), \tag{A5}$$
$$\frac{\partial v_1}{\partial t} = D_1\frac{\partial^2 v_1}{\partial x^2} + \gamma(g(u_1, v_1) + \eta(v_2 - v_1)), \tag{A6}$$
$$\frac{\partial u_2}{\partial t} = D_2\frac{\partial^2 u_2}{\partial x^2} + \gamma(f(u_2, v_2) + \eta(u_1 - u_2)), \tag{A7}$$
$$\frac{\partial v_2}{\partial t} = D_3\frac{\partial^2 v_2}{\partial x^2} + \gamma(g(u_2, v_2) + \eta(v_1 - v_2)), \tag{A8}$$

where $f(u_i, v_i)$ and $g(u_i, v_i)$ are defined as per equations (5) and (6), respectively. It is important to note that we have consistently adopted the value $\gamma = 1$ throughout the discussion, as it is essential for η to serve as the exclusive constant governing the coupling strength.

Appendix B: Numerical scheme convergence

To illustrate the accuracy and convergence of our numerical codes, we simulate the system four times for $\eta = 0$ (giving each solution curve a name, e_i, $i = 0, 1, \ldots, 3$) with refined time steps and grid nodes, see Table II.

	Δt	n_x	t_{final}
e_0	0.01	200	2045
e_1	0.00825	264	1974
e_2	0.0065	328	1902
e_3	0.00475	392	1804

Table II: Time step, grid nodes and the corresponding duration (t_{final}) required for the establishment of a stable pattern for the solution curves e_i.

Visually, the numerical scheme provided consistent behaviour of the system for all refined grid sizes and time steps, when $\eta = 0$. To evidence this we interpolate the results onto the same grids and then extract that absolate maximum differences between them, illustrated in Fig. 8. Clearly, we see that as the space and time are refined the differences between the curves

also reduce. In a similar vein, the behaviour is corroborated across a range of values for η, specifically, $(0, 0.17, 0.43, 3.77, 10)$.

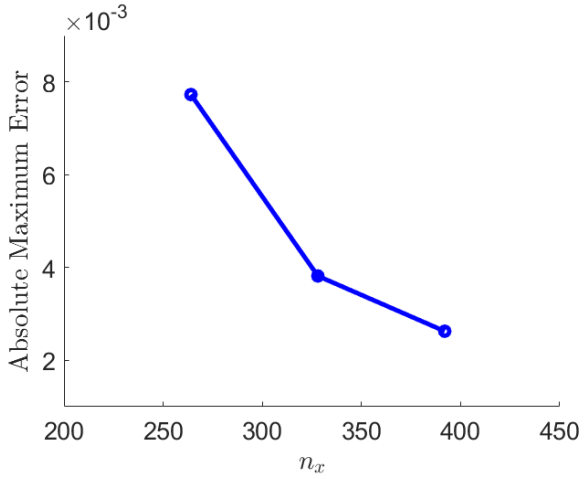

Figure 8: Absolute maximum error differences between the solution curves e_i and e_{i-1} for $i = 1, 2, \ldots, 5$ provided in Table II.

Appendix C: Linear stability analysis of the individual layers

I. without diffusion

We require system equations (A1) and (A2) to be stable without diffusion and coupling, thus, we substitute solution (7) into

$$\frac{du_i}{dt} = f(u_i, v_i), \tag{C1}$$
$$\frac{dv_i}{dt} = g(u_i, v_i). \tag{C2}$$

Upon linearising about ω_{u_i} and ω_{v_i} we derive that the perturbation must satisfy

$$(\lambda \mathbf{I}_2 - \mathbf{J}_i)\, \boldsymbol{\omega}_i = \mathbf{0}, \tag{C3}$$

where,

$$\mathbf{J}_i = \begin{pmatrix} f_{u_i} & f_{v_i} \\ g_{u_i} & g_{v_i} \end{pmatrix}\Bigg|_{\boldsymbol{u}_{i_0}}. \tag{C4}$$

We note that because the kinetics are the same on both layers the partial derivatives are independent of i, e.g. $f_{u_1} = f_{u_2}$ and thus we have $\mathbf{J}_1 = \mathbf{J}_2 = \mathbf{J}$. Thus, the characteristic polynomial of (C3) is given by

$$s(\lambda) = \lambda^2 - (f_u + g_v)\lambda + f_u g_v - g_u f_v = 0,$$

independent of i. In order for system (C1) and (C2) to be stable, it is necessary to have a negative trace ($c_1 = f_u + g_v < 0$) and a positive determinant ($c_2 = f_u g_v - g_u f_v > 0$) of $\mathbf{J}$ [1].

For the Schnakenberg kinetics (5) and (6) with parameters $a > 0$ and $b > 0$, we have

$$c_1 = \frac{b-a}{a+b} - (a+b)^2, \tag{C5}$$
$$c_2 = (a+b)^2, \tag{C6}$$

for all a, b. Since $c_2 > 0$ for all $a, b > 0$ the Turing parameter region is controlled by the sign of c_1, which can assuredly become negative in the case that $b = a$. Thus, there is a parameter region under which system (A1) and (A2) is stable without diffusion and coupling.

II. with diffusion

The dimensionless system (A1) and (A2) without coupling but with diffusion is provided by

$$\frac{\partial u_i}{\partial t} = \frac{\partial^2 u_i}{\partial x^2} + \gamma f(u_i, v_i), \tag{C7}$$
$$\frac{\partial v_i}{\partial t} = d_i \frac{\partial^2 v_i}{\partial x^2} + \gamma g(u_i, v_i), \tag{C8}$$

where f and g are given by (5) and (6), $d_1 = D_1$, $d_2 = D_3/D_2$ and $\gamma = 1$. Again, upon linearising by substituting solution (7) with $\boldsymbol{\epsilon}_i = \boldsymbol{\omega}_i \exp(\lambda t)\cos(kx)$, where $k = n\pi/L$ is the wave number with $n \in \mathbb{Z}$ that satisfies the no-flux boundary conditions on $[0, L]$, we get

$$(\lambda \mathbf{I}_2 - \mathbf{J}_{d,i})\, \boldsymbol{\omega}_i = \mathbf{0}, \tag{C9}$$

where $\mathbf{J}_{d,i} = k^2 \mathbf{D}_i - \mathbf{J}$, $\mathbf{D}_i = diag(1, d_i)$. Based on the diffusion-driven instability phenomena, our systems (C7) and (C8) must be unstable for each layer to pattern separately. Accordingly, we verify our system's trace and determinant for instability [1]

$$trace(\mathbf{J}_{d,i}) = -k^2(1 + d_i) + (f_u + g_v), \tag{C10}$$
$$|\mathbf{J}_{d,i}| = k^4 d_i - k^2(g_v + d_i f_u) + (f_u g_v - g_u f_v). \tag{C11}$$

As the trace (C10) is always negative, we need $|\mathbf{J}_{d,i}| > 0$ implying

$$k_-^2 < k^2 < k_+^2, \tag{C12}$$

where

$$k_\pm^2 = \frac{(g_v + d_i f_u) \pm \sqrt{(g_v + d_i f_u)^2 - 4 d_i (f_u g_v - g_u f_v)}}{2 d_i}. \tag{C13}$$

This requires that the domain be sufficiently large to enable the emergence of an unstable mode, thus defining the patterning domain. It follows that for k_+^2 to be both real and positive, we arrive at the inequality

$$g_v + d_i f_u > 2\sqrt{d_i(f_u g_v - g_u f_v)} > 0, \tag{C14}$$

and hence the constants

$$c_{8,1} = g_v + D_1 f_u, \tag{C15}$$
$$c_{9,2} = g_v + (D_3/D_2) f_u, \tag{C16}$$

are positive.

Appendix D: Stability criteria

Our objective is to illustrate the Routh-Hurwitz (RH) stability criterion by investigating it in detail for quartic polynomials,

$$p(\lambda) = \lambda^4 + \alpha_3\lambda^3 + \alpha_2\lambda^2 + \alpha_1\lambda + \alpha_0.$$

The RH criterion [46, 47] provides the necessary and sufficient conditions for a stable linear system. The necessary condition is that all the coefficients of the polynomial must be positive and none of the coefficients must be zero. The sufficient condition is based on an array, called the Routh array, constructed from the coefficients of the characteristic polynomial that requires all the elements of the first column of the Routh array to have the same sign. Furthermore, the RH criterion informs us that the number of roots of the characteristic polynomial with positive real parts (indicating an unstable steady state) is equal to the number of sign changes of the coefficients in the first column of the array.

The Routh array (Table III) is constructed for $p(\lambda)$ as described in [47]. Explicitly, the initial two rows of the table display the coefficients of the two polynomials, organised in descending order of degree terms

$$p_1(\lambda) = \lambda^4 + \alpha_2\lambda^2 + \alpha_0,$$
$$p_2(\lambda) = \alpha_3\lambda^3 + \alpha_1\lambda,$$

which contain solely the terms with even degrees and odd degrees of $p(\lambda)$. A polynomial, $p_3(\lambda)$, is defined as the remainder of the division of polynomial $p_1(\lambda)$ by $p_2(\lambda)$, thus, so that $p_3(\lambda) = p_1(\lambda) - q_1(\lambda)p_2(\lambda)$, where $q_1(\lambda) = \lambda/\alpha_3$ represents the quotient. The third row of Table III contains the coefficients of the remainder $p_3(\lambda) = ((\alpha_3\alpha_2 - \alpha_1)/\alpha_3)\lambda^2 + \alpha_0$. By following the same process, we can define polynomials $p_m(\lambda) = p_{m-2}(\lambda) - q_m(\lambda)p_{m-1}(\lambda)$, which represents the remainder of the polynomial $p_{m-2}(\lambda)$ when divided by $p_{m-1}(\lambda)$, where $q_m(\lambda) = \dfrac{r_{m-2}}{r_{m-1}}\lambda$ is the quotient with r_m being the leading coefficient of p_m.

The $p_m(\lambda)$ polynomials display a sequence where they alternate between being even and odd, with each polynomial having a lower order than the previous one. The Routh array includes the coefficients of these polynomials, excluding any coefficients that are consistently zero. The coefficients of the polynomials p_m can be determined using a straightforward method illustrated in Table III. To retrieve the ν_n component of p_m, one can determine the negative determinant of a square matrix that is formed with the ν_1 and ν_{n+1} components taken from p_{m-2} and p_{m-1}, respectively, as the first and second columns of the matrix, and then dividing the result by the ν_1 component of p_{m-1}, while treating the missing components as zero. The labels on the left side of the Routh array indicate the highest power of λ of the polynomials p_m.

	ν_1	ν_2	ν_3
$p_1:\lambda^4$	1	α_2	α_0
$p_2:\lambda^3$	α_3	α_1	0
$p_3:\lambda^2$	$\dfrac{-\begin{vmatrix}1 & \alpha_2\\ \alpha_3 & \alpha_1\end{vmatrix}}{\alpha_3} = \beta_1$	$\dfrac{-\begin{vmatrix}1 & \alpha_0\\ \alpha_3 & 0\end{vmatrix}}{\alpha_3} = \alpha_0$	$\dfrac{-\begin{vmatrix}1 & 0\\ \alpha_3 & 0\end{vmatrix}}{a_3} = 0$
$p_4:\lambda^1$	$\dfrac{-\begin{vmatrix}\alpha_3 & \alpha_1\\ \beta_1 & \alpha_0\end{vmatrix}}{\beta_1} = \gamma_1$	$\dfrac{-\begin{vmatrix}\alpha_3 & 0\\ \beta_1 & 0\end{vmatrix}}{\beta_1} = 0$	$\dfrac{-\begin{vmatrix}\alpha_3 & 0\\ \beta_1 & 0\end{vmatrix}}{\beta_1} = 0$
$p_5:\lambda^0$	$\dfrac{-\begin{vmatrix}\beta_1 & \alpha_0\\ \gamma_1 & 0\end{vmatrix}}{\gamma_1} = \alpha_0$	$\dfrac{-\begin{vmatrix}\beta_1 & 0\\ \gamma_1 & 0\end{vmatrix}}{\gamma_1} = 0$	$\dfrac{-\begin{vmatrix}\beta_1 & 0\\ \gamma_1 & 0\end{vmatrix}}{\gamma_1} = 0$

Table III: Routh array.

In Table III, after simplifying we have $\beta_1 = \dfrac{(\alpha_3\alpha_2 - \alpha_1)}{\alpha_3}$, and $\gamma_1 = \dfrac{\alpha_1\alpha_2\alpha_3 - \alpha_1^2 - \alpha_3^2\alpha_0}{\alpha_2\alpha_3 - \alpha_1}$. Thus, according to the Routh-Hurwitz stability criterion, it is necessary to confirm that the four coefficients (α_3, α_2, α_1, and α_0) and the two additional elements (β_1 and γ_1), which result from a particular combination of the coefficients, are positive in order to ascertain the stability of the linear system.

Appendix E: Explicit coefficients for the coupled system without diffusion

In Section V, we derived that equation (13) was a quartic polynomial in λ. In this section, we provide the coefficients for each of the terms. Explicitly, for the

parameters under consideration, the four coefficients

$$\begin{aligned} y_{3_0} &= 4\eta + 2.34, \\ y_{2_0} &= 4\eta^2 + 7.03\eta + 5.58, \\ y_{1_0} &= 4.69\eta^2 + 11.15\eta + 4.93, \\ y_{0_0} &= 8.41\eta^2 + 4.93\eta + 4.42, \end{aligned}$$

are all positive as $\eta > 0$ and the two additional elements

$$\begin{aligned} y_{\beta_0} &= 4\eta^2 + 5.86\eta + 3.48, \\ y_{\gamma_0} &= \frac{1}{y_{\beta_0}} \left(18.74\eta^4 + 38.42\eta^3 + 61.91\eta^2 \right. \\ &\quad \left. + 38.39\eta + 6.76\right), \end{aligned}$$

are also positive with $\eta > 0$.

Appendix F: Explicit coefficients for the coupled system with diffusion

Equations (17) through (22) in Section VI are included in this appendix. It contains the explicit coefficient values as a function of (h, η) for these equations. You can also find these equations on the GitHub link mentioned in the Numerical code section.

$$\begin{aligned} y_3 &= 891h + (4\eta + 2.34), \\ y_2 &= 74890h^2 + (2673\eta + 338.49)h + (4\eta^2 + 7.03\eta \\ &\quad + 5.58), \\ y_1 &= 1674000h^3 + (149780\eta - 33497)h^2 + (1782\eta^2 \\ &\quad + 676.97\eta + 1047.20)h + (4.69\eta^2 + 11.15\eta + 4.93), \\ y_0 &= 1600000h^4 + (1674000\eta - 1455519)h^3 + (34850\eta^2 \\ &\quad - 33497\eta + 96758)h^2 + (-1410.50\eta^2 + 1047.20\eta \\ &\quad - 1482.80)h + (8.41\eta^2 + 4.93\eta + 4.42), \\ y_\beta &= \frac{1}{y_3} \left[65052990h^3 + (2531423\eta + 510540)h^2 \right. \\ &\quad + (12474\eta^2 + 13202\eta + 4715)h + (16\eta^3 + 32.80\eta^2 \\ &\quad \left. + 27.62\eta + 8.14)\right], \\ y_\gamma &= \frac{1}{(y_2 y_3 - y_1)} \left[1.07e^{14}h^6 + (1.26e^{13}\eta - 1.75e^{11})h^5 \right. \\ &\quad + (4.76e^{11}\eta^2 + 8.77e^{10}\eta - 1.18e^{10})h^4 + (6.13e^9\eta^3 \\ &\quad + 5.74e^9\eta^2 + 2.66e^9\eta + 1.49e^9)h^3 + (24067548\eta^4 \\ &\quad + 5.81e^7\eta^3 + 5.47e^7\eta^2 + 3.61e^7\eta + 9.32e^6)h^2 \\ &\quad + (28512\eta^5 + 1.50e^5\eta^4 + 2.38e^5\eta^3 + 2.39e^5\eta^2 \\ &\quad + 1.22e^5\eta + 2.14e^4)h + (74.97\eta^5 + 197.59\eta^4 \\ &\quad \left. + 337.65\eta^3 + 298.58\eta^2 + 116.97\eta + 15.84)\right]. \end{aligned}$$

Since $h = k^2$, $k > 0$, and $\eta > 0$, it follows that $y_3 > 0$, $y_2 > 0$, and consequently $y_\beta > 0$. On the other hand, y_1 and y_γ (Fig. 3(c) and 3(f)) do not show any discernible patterns, while y_0 (Fig. 3(d)) reveals a distinct region in (k, η) that displays pattern formation.

NUMERICAL CODE

The necessary equations can be located in the appendices, while the corresponding code containing these equations is available on GitHub at `https://github.com/mahaksn/Linear-Coupling`.

ACKNOWLEDGEMENTS

The primary author would like to express gratitude for the financial support provided through the INSPIRE fellowship by the Department of Science and Technology, Government of India, India. Also, this work is supported by Vellore Institute of Technology, Vellore under a SEED grant (Sanction Order No. SG20230081).

[1] J. D. Murray. *Mathematical biology: II: spatial models and biomedical applications*, volume 18. Springer, 2003.

[2] A. M. Turing. The chemical basis of morphogenesis. *Philos. Trans. R. Soc., B*, 237:37–72, 1952.

[3] S. Kondo and T. Miura. Reaction-diffusion model as a framework for understanding biological pattern formation. *Science*, 329:1616–20, 2010.

[4] S. W. Cho, S. Kwak, T. E. Woolley, M. J. Lee, E. J. Kim, R. E. Baker, H. J. Kim, J. S. Shin, C. Tickle, P. K. Maini, and H. S. Jung. Interactions between Shh, Sostdc1 and Wnt signaling and a new feedback loop for spatial patterning of the teeth. *Development*, 138:1807–1816, 2011.

[5] J. D. Glover, K. L. Wells, F. Matthäus, K. J. Painter, W. Ho, J. Riddell, J. A. Johansson, M. J. Ford, C. A. B. Jahoda, V. Klika, et al. Hierarchical patterning modes orchestrate hair follicle morphogenesis. *PLoS Biol.*, 15(7):e2002117, 2017.

[6] W. K. W. Ho, L. Freem, D. Zhao, K. J. Painter, T. E. Woolley, E. A. Gaffney, M. J. McGrew, A. Tzika, M. C. Milinkovitch, P. Schneider, et al. Feather arrays are patterned by interacting signalling and cell density waves. *PLoS Biol.*, 17(2):e3000132, 2019.

[7] J. D. Glover, Z. R. Sudderick, B. B. J. Shih, C. Batho-Samblas, L. Charlton, A. L. Krause, C. Anderson, J. Riddell, Ad. Balic, J. Li, et al. The developmental basis of fingerprint pattern formation and variation. *Cell*, 186(5):940–956, 2023.

[8] VV. Castets, E. Dulos, J. Boissonade, and P. Kepper. Experimental evidence of a sustained standing turing-type nonequilibrium chemical pattern. *Phys. Rev. Lett.*, 64:2953–2956, 1990.

[9] T. E. Woolley. *50 Visions of Mathematics*, chapter 48: Mighty Morphogenesis. Oxford University Press, 2014.

[10] P. K. Maini, T. E. Woolley, R. E. Baker, E. A. Gaffney, and S. S. Lee. Turing's model for biological pattern formation and the robustness problem. *Interface Focus*, 2(4):487–496, 2012.

[11] P. K. Maini, T. E. Woolley, E. A. Gaffney, and R. E. Baker. *The Once and Future Turing*, chapter 15: Biological pattern formation. Cambridge University Press, 2016.

[12] J. W. Moore, T. C. Dale, and T. E. Woolley. Modeling polarity-driven laminar patterns in bilayer tissues with mixed signaling mechanisms. *SIAM Journal on Applied Dynamical Systems*, 22(4):2945–2990, 2023.

[13] S. Sinha and S. Sridhar. *Patterns in excitable media: Genesis, dynamics, and control.* CRC Press, 2014.

[14] R. Sekine, T. Shibata, and M. Ebisuya. Synthetic mammalian pattern formation driven by differential diffusivity of nodal and lefty. *Nat. Commun.*, 9(1):5456, 2018.

[15] I. R. Epstein, I. B. Berenstein, M. Dolnik, V. K. Vanag, L. Yang, and A. M. Zhabotinsky. Coupled and forced patterns in reaction–diffusion systems. *Philos. Trans. R. Soc., A*, 366(1864):397–408, 2008.

[16] L. Yang, M. Dolnik, A. M. Zhabotinsky, and I. R. Epstein. Spatial resonances and superposition patterns in a reaction-diffusion model with interacting turing modes. *Phys. Rev. Lett.*, 88(20):208303, 2002.

[17] L. Yang and I. R. Epstein. Symmetric, asymmetric, and antiphase turing patterns in a model system with two identical coupled layers. *Phys. Rev. E*, 69(2):026211, 2004.

[18] A. Diez, A. L. Krause, P. K. Maini, E. A. Gaffney, and S. Seirin-Lee. Turing pattern formation in reaction-cross-diffusion systems with a bilayer geometry. *Bull. Math. Biol.*, 86(2):13, 2024.

[19] L. Yang and I. R. Epstein. Oscillatory turing patterns in reaction-diffusion systems with two coupled layers. *Phys. Rev. Lett.*, 90(17):178303, 2003.

[20] I. Berenstein, M. Dolnik, L. Yang, A. M. Zhabotinsky, and I. R. Epstein. Turing pattern formation in a two-layer system: superposition and superlattice patterns. *Phys. Rev. E*, 70(4):046219, 2004.

[21] L. Yang, M. Dolnik, A. M. Zhabotinsky, and I. R. Epstein. Turing patterns beyond hexagons and stripes. *Chaos: An Interdisciplinary Journal of Nonlinear Science*, 16(3):037114, 2006.

[22] D. G. Míguez, M. Dolnik, I. Epstein, and Alberto P Munuzuri. Interaction of chemical patterns in coupled layers. *Phys. Rev. E*, 84(4):046210, 2011.

[23] K. Konishi and N. Hara. Stabilization of a spatially uniform steady state in two systems exhibiting turing patterns. *Phys. Rev. E*, 97(5):052201, 2018.

[24] A. J. Catllá, A. McNamara, and C. M. Topaz. Instabilities and patterns in coupled reaction-diffusion layers. *Phys. Rev. E*, 85(2):026215, 2012.

[25] A. M. Rucklidge, M. Silber, and A. C. Skeldon. Three-wave interactions and spatiotemporal chaos. *Phys. Rev. Lett.*, 108(7):074504, 2012.

[26] J. K. Castelino, D. J. Ratliff, A. M. Rucklidge, P. Subramanian, and C. M. Topaz. Spatiotemporal chaos and quasipatterns in coupled reaction–diffusion systems. *Phys. D (Amsterdam, Neth.)*, 409:132475, 2020.

[27] A. L. Krause, V. Klika, J. Halatek, P. K. Grant, T. E. Woolley, N. Dalchau, and E. A. Gaffney. Turing patterning in stratified domains. *Bull. Math. Biol.*, 82(10):136, 2020.

[28] K. R. Swanson, E. C. Alvord Jr, and J. D. Murray. A quantitative model for differential motility of gliomas in grey and white matter. *Cell Proliferation*, 33(5):317–329, 2000.

[29] J. Belmonte-Beitia, T. E. Woolley, J. G. Scott, P. K. Maini, and E. A. Gaffney. Modelling biological invasions: Individual to population scales at interfaces. *J. Theor. Biol.*, 334:1 – 12, 2013.

[30] L. Ji and Q. S. Li. Turing pattern formation in coupled reaction-diffusion system with distributed delays. *The Journal of Chemical Physics*, 123(9):94509, 2005.

[31] K. Kyttä, K. Kaski, and R. A. Barrio. Complex turing patterns in non-linearly coupled systems. *Phys. A (Amsterdam, Neth.)*, 385(1):105–114, 2007.

[32] X. Z. Li, Z. G. Bai, Y. Li, Y. F. He, and K. Zhao. Numerical simulation and analysis of complex patterns in a two-layer coupled reaction diffusion system. *Chin. Phys. B*, 24(4):048201, 2015.

[33] G. Saxena, A. Prasad, and R. Ramaswamy. Amplitude death: The emergence of stationarity in coupled nonlinear systems. *Phys. Rep.*, 521(5):205–228, 2012.

[34] A. Koseska, E. Volkov, and J. Kurths. Transition from amplitude to oscillation death via turing bifurcation. *Phys. Rev. Lett.*, 111(2):024103, 2013.

[35] W. Zou, D. V. Senthilkumar, A. Koseska, and J. Kurths. Generalizing the transition from amplitude to oscillation death in coupled oscillators. *Phys. Rev. E*, 88(5):050901, 2013.

[36] A. Gierer and H. Meinhardt. A theory of biological pattern formation. *Biological Cybernetics*, 12:30–39, 01 1972.

[37] P. K. Maini and T. E. Woolley. *The Turing Model for Biological Pattern Formation*, pages 189–204. Springer, 2019.

[38] J. Schnakenberg. Simple chemical reaction systems with limit cycle behaviour. *J. Theor. Biol.*, 81(3):389–400, 1979.

[39] S. J. Ruuth. Implicit-explicit methods for reaction-diffusion problems in pattern formation. *Journal of Mathematical Biology*, 34(2):148–176, 1995.

[40] U. M. Ascher, S. J. Ruuth, and B. T. R. Wetton. Implicit-explicit methods for time-dependent partial differential equations. *SIAM Journal on Numerical Analysis*, 32(3):797–823, 1995.

[41] M. Kamrani and S. M. Hosseini. The role of coefficients of a general spde on the stability and convergence of a finite difference method. *Journal of Computational and Applied Mathematics*, 234(5):1426–1434, 2010.

[42] G. E. Zouraris. Crank–nicolson finite element approximations for a linear stochastic fourth order equation with additive space-time white noise. *SIAM Journal on Numerical Analysis*, 56(2):838–858, 2018.

[43] J. W. Thomas. *Numerical partial differential equations: finite difference methods*, volume 22. Springer Science & Business Media, 2013.

[44] A. Madzvamuse and A. H. Chung. Fully implicit time-stepping schemes and non-linear solvers for systems of reaction–diffusion equations. *Applied Mathematics and Computation*, 244:361–374, 2014.

[45] T. E. Woolley. *Spatiotemporal Behaviour of Stochastic and Continuum Models for Biological Signalling on Stationary and Growing Domains*. PhD thesis, University of Oxford, 2011.

[46] A. A. Kumar. *Control systems*. PHI Learning Pvt. Ltd., 2014.

[47] M. Bodson. Explaining the routh–hurwitz criterion: A tutorial presentation [focus on education]. *IEEE Control Systems Magazine*, 40(1):45–51, 2020.